

Systematic error analysis of the Symmetric Hybrid ring design in the storage-ring proton electric dipole moment experiment

Zhanibek Omarov^{1,2}, Selcuk Hacıömeroğlu², and Yannis K. Semertzidis^{1,2}

¹Department of Physics, Korea Advanced Institute of Science and Technology (KAIST), Daejeon 34141, Republic of Korea

²Center for Axion and Precision Physics Research, Institute for Basic Science (IBS/CAPP), Daejeon 34051, Republic of Korea

June 2020

Abstract

We introduce a symmetric hybrid ring design for the storage ring proton EDM experiment, and analyze its crucial systematics. Spin-based alignment is introduced in order to provide a tool for precision alignment of electric bending plates. Overall, we find that the main systematic errors are relaxed by several orders of magnitude.

1 Introduction

The storage ring EDM method targets EDM sensitivity below $10^{-29} e\cdot\text{cm}$. We claim that this sensitivity is achievable with existing technology due to significantly relaxed alignment requirements. This paper aims to address most prominent systematic errors from the initial discussion of the storage ring proton EDM experiment [1] and the follow-up hybrid ring variant of the same ring [2]. Hybrid-ring variant has been a major upgrade over the original all-electric variant. This work focuses on the symmetric modification of the hybrid ring which relaxes alignment requirements by a few orders of magnitude. All the improvements achieved by the hybrid variant are preserved here.

Here, we will focus on the most important systematic issues and methods of their remediation. The systematic issues to be covered in this text are:

1. Vertical velocity in the bending sections
2. Dipole vertical E -field
3. Geometrical phase

The ring geometry will be discussed thoroughly first, followed by detailed analysis of each systematic issue. Interpretation and relevant analysis will be given accordingly when necessary.

2 Methods

2.1 Ring Geometrical Structure

The 800m Symmetric ring was designed to maximize electrical bending sections. To do so, we had decided to put 600m of bending sections and 200m of straight sections. The Symmetric ring is composed of:

1. Electrical Bending Section. The bending section is composed of 1 deflector with an arc length of $360^\circ/48 = 7.5^\circ$ and a bending radius of $R_0 = 95.49$ m. Each deflector is 12.5 m long. Electrical bending sections comprise 600m in ring circumference.
2. Magnetic Quadrupole Section. Each quadrupole is 40 cm in length, padded with 1.88 m empty sections. The strength of the quadrupoles is $k = \pm 0.2$ T/m so that the ring is below transition. The slip factor as a function of quad strength could be found in Figure 3

To make a FODO cell, we take section 1, put a Focusing section 2, follow with another section 1, finish it with Defocusing section 2. A single FODO is illustrated on Figure 1. The entire ring is made up with 24 FODO sections, making up to 800 m in circumference. The beta functions are given in Figure 4

2.2 Polarity switch and Counter-rotating beams

We define the polarity switch to be the act of switching the direction of the currents in the (de)focusing sections. Focusing sections being current driven magnetic quadrupoles, the act of reversing polarity would make a focusing quad to be defocusing. Equivalently, we shift the phase of the beta functions for both clockwise (CW) and counter-clockwise (CCW) beams. This technique improves the sensitivity and cancels some important systematic errors. Illustration of the CCW-CW injections is shown in Figure 2

Radial polarization indicates that the initial spin direction of the beam is directed radially outwards both in clockwise (CW) and counter-clockwise (CCW) directions. That is, spins begin pointing away from the center of the ring for both CW and CCW beam directions.

Longitudinal polarization means that the initial spins are aligned with the momentum. Hence, CCW and CW have their spins pointing onto one another. Different polarization directions are differently sensitive to systematics; hence, having bunches polarized differently would give us another leverage to combat systematic issues.

2.3 High precision tracking

Runge-Kutta family integrator (5th order, adaptive step size [3]) was used in order to perform simulations throughout this work. Both beam and spin dynamics are fully tracked numerically.

$$\frac{d\vec{\beta}}{TDD} = \frac{e}{m\gamma c} \left[\vec{E} + c\vec{\beta} \times \vec{B} - \beta(\vec{\beta} \cdot \vec{E}) \right] \quad (1)$$

Spin is tracked via BMT equation [4],

$$\frac{d\vec{S}}{dt} = \frac{e}{m} \vec{S} \times \left[\left(a + \frac{1}{\gamma} \right) \vec{B} - \frac{a\gamma}{\gamma+1} \vec{\beta}(\vec{\beta} \cdot \vec{B}) - \left(a + \frac{1}{\gamma+1} \right) \frac{\vec{\beta} \times \vec{E}}{c} \right] \quad (2)$$

No matrix approximations were used in order to keep up with precision requirements. An energy benchmark for the reference particle at magic momentum is given in Figure 5.



Figure 1: Schematic view of a single FODO cell. Legend: F-Focusing quadrupole, D-Defocusing quadrupole, S-Straight section, E-Electric bending section.

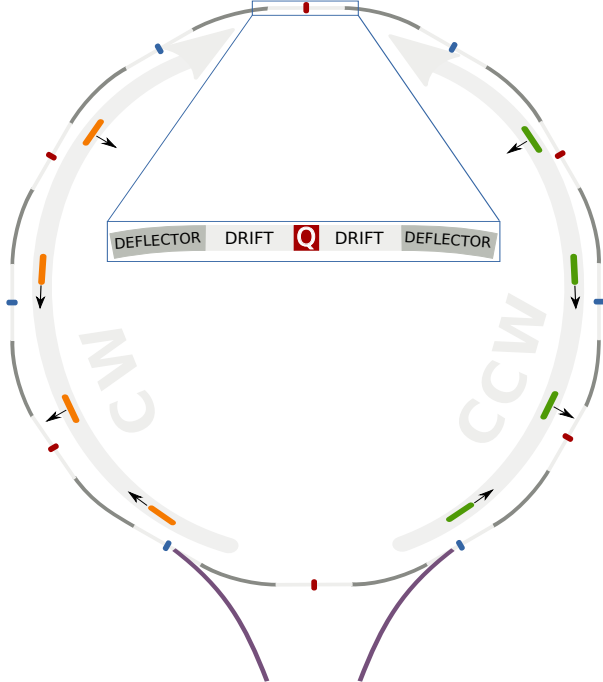


Figure 2: Schematic top view of the symmetric ring. Both CW and CCW beams have longitudinally, radially, and vertically polarized bunches. Blue and red correspond to focusing and defocusing quads. Naturally, CW and CCW beams see opposite focusing effect from magnetic quads. The actual number of FODO sections is 24.

3 Systematic Errors

3.1 Vertical Velocity

Vertical velocity systematic originates from the

$$(\vec{\beta} \times \vec{E})_s = \beta_y \times E_x$$

term in the BMT equation Equation (2) (x, y, s refer to FS coordinate system, with x pointing out of the ring center, y pointing vertically, s pointing in the direction of the motion). Naturally, only S_x radial polarization is sensitive to this term. However, this effect is still crucial in the longitudinal polarization. Any longitudinal polarized beam would exhibit some oscillations in the plane of the ring projecting little of the spin radially. Little oscillating radial spin component could cause a trouble even if the oscillation amplitude is only 1/1000 of the total spin.

The simplest condition in which this systematic manifests itself is quad misalignment. One quad misaligned vertically by a 1 μm is enough of a condition to cause a false EDM signal. Single vertically misaligned quad produces an imbalance in vertical velocities of the particle: average vertical velocity in bending sections is no longer zero. The average vertical velocity over the entire ring is exactly zero by definition; however, it could be non-zero if averaged over bending sections only (E_x field regions). As the other half of the velocity is compensated in the quads. Formally,

$$\langle \beta_y \rangle_{\text{straight}} + \langle \beta_y \rangle_{\text{bending}} \equiv 0$$

This systematic has been especially prominent in the original 4-fold symmetric hybrid ring design [2] (Figure 6), where misaligned quads are not equivalent (symmetric) and this effect is even more pronounced. To illustrate this at hand, let us vertically misalign one quad at a time by 1 μm . Vertical spin precession rate as a function of index of the misaligned quad is given in Figure 7. This tells us that only the quads at the very symmetrical locations in the 4-fold symmetric ring are insensitive to corresponding misalignments.

This has lead us to the idea to make all the quads maximally symmetric with respect to each other. Hence, the idea to make the symmetric ring was born (Figure 2). The vertical velocity systematic manifests itself few orders of magnitude less in the symmetric design Figure 8. As it is seen from the figure, vast improvement in the background vertical precession rate can achieved by placing the quads symmetrically with respect to each other.

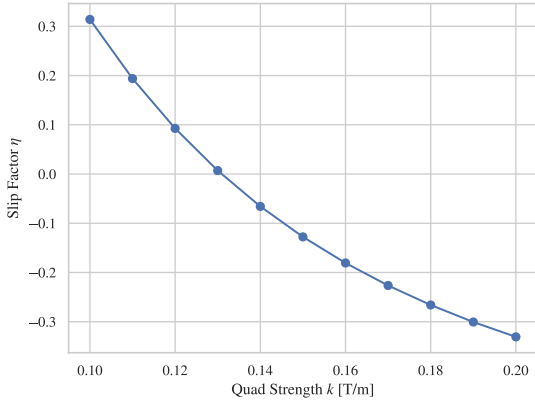


Figure 3: The slip factor η is obtained from evaluating $\frac{dt}{t} = \eta \frac{dp}{p}$ per turn via numerical tracking.

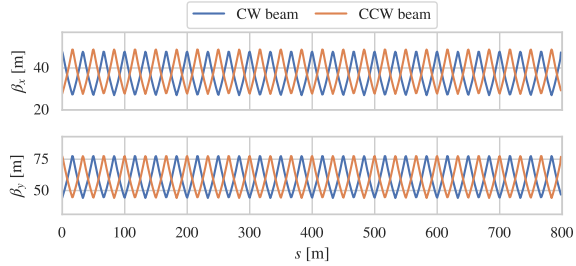


Figure 4: Beta functions along the ring. The results were obtained via numerical tracking.

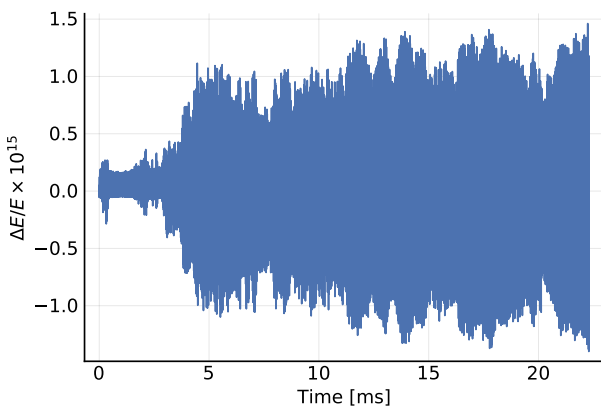


Figure 5: Relative energy conservation for a reference reference particle. The relative particle energy $\Delta E/E$ is conserved to up to the floating point precision 1×10^{-15} .

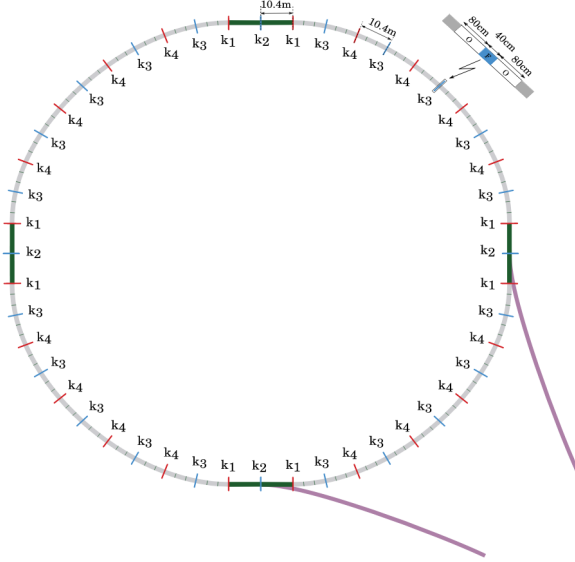


Figure 6: 4-fold symmetric ring design, presence of the long straight sections reduce the number of symmetric points (adapted from [1])

3.2 Dipole E -field

Dipole E -field systematic originates from the

$$(\vec{\beta} \times \vec{E})_x = \beta_s \times E_y$$

term in Equation (2). Non-zero E_y could arise due to some tilt in the deflector plates. This creates an EDM-like signal for one of the counter rotating beams. However, a true EDM-signal would cause the vertical spin precession in opposite directions for CW and CCW beams. Hence, having CW and CCW beams is critical to combat this systematic, as dipole E -field creates opposite to true EDM signal for each direction. Therefore, taking difference of the precession rates for CW and CCW beams gives us true EDM signal. Formally,

$$\left(\frac{dS_y}{dt} \right)_{\text{EDM}} = \frac{1}{2} \left(\frac{dS_y}{dt} \right)_{\text{CW}} - \frac{1}{2} \left(\frac{dS_y}{dt} \right)_{\text{CCW}}$$

Dipole E -field creates discernible from EDM signal with CW and CCW beams.

Dipole E -field can happen due to some tilt in the bending plates. Let us assume a normal distribution of tilts with $\sigma = 0.1$ mrad. Now, each bending section being randomly tilted, it creates a net non-zero dipole E -field in the ring. This creates some precession in CW and CCW beams Figure 9.

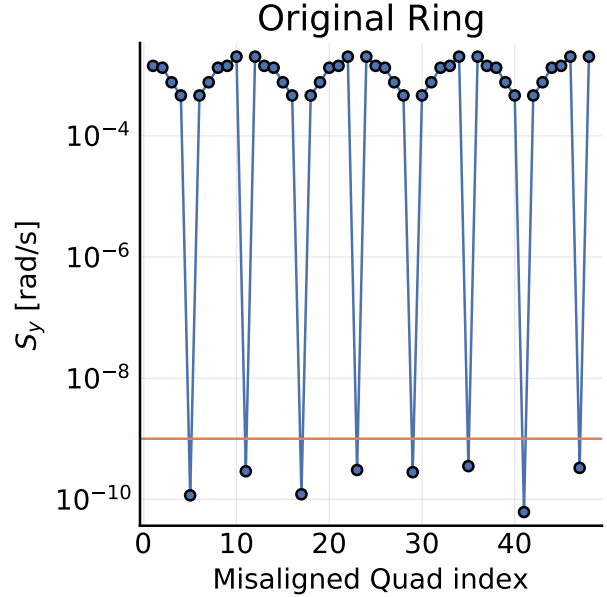


Figure 7: Vertical spin precession rate vs. index of the 1 μm misaligned quad along the azimuth. The original 4-fold symmetric ring design is used (Figure 6 [1]). Dips of the graph correspond 1'30", 4'30", 7'30", 10'30" o'clock, and points in between shown in Figure 6. Irregularities of the points at low rates are due to the inability to determine the exact precession rate from simulation results. Hence, the points only show upper limit of the possible vertical precession rate, actual rates could be lower. The orange line corresponds to the target EDM sensitivity

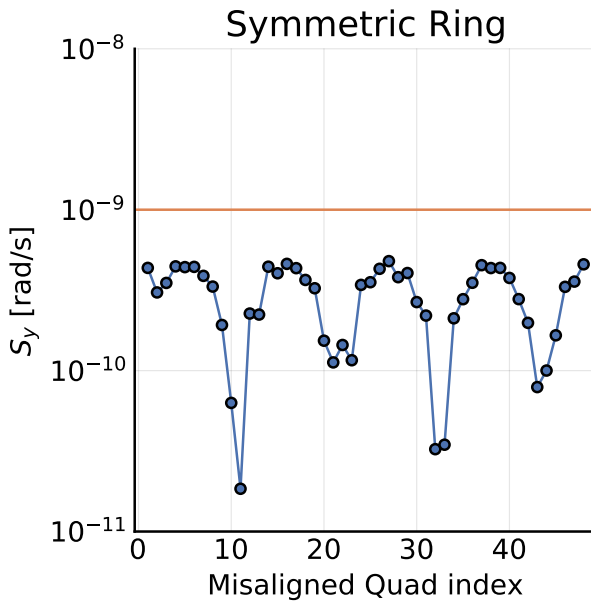


Figure 8: Vertical spin precession rate vs. index of the $1\text{ }\mu\text{m}$ misaligned quad along the azimuth. Irregularities of the points are due to the inability to determine the exact precession rate from the simulation results. Hence, the points only show upper limit of the possible vertical precession rate, actual rates could be lower. The orange line corresponds to the target EDM sensitivity

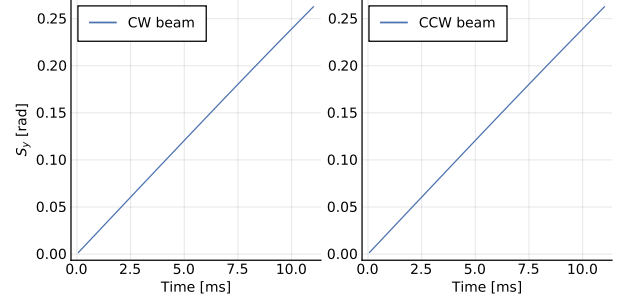


Figure 9: Vertical spin component vs. time. Opposite directions (CW and CCW) precess in the same direction (lab frame). EDM signal could be discerned by looking at the difference of the precessions.

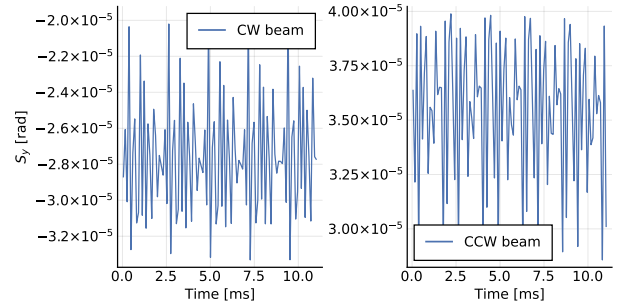


Figure 10: Vertical spin component vs. time. Opposite directions (CW and CCW) stop precessing if compensating trim field is setup at any position in the ring.

We can compensate for this precession by applying opposite trimming dipole field until no visible precession is seen in both directions Figure 10. This trim field could be applied anywhere in the ring as long as it averages out the net E field to zero.

3.3 Geometrical Phase — Quadrupole Sections

Geometrical phase effect [5–7] is an extra phase obtained due to non-commutativity of the successive rotations in the context of the storage ring EDM experiment. Its signature is the square dependence of the precession rate against rotation amplitudes. A typical way to create a background vertical precession rate is to randomly misalign quadrupoles both horizontally and vertically. Then, the vertical precession rate should follow these misalignments as the product of their amplitudes.

In order to observe the effect we may proceed by

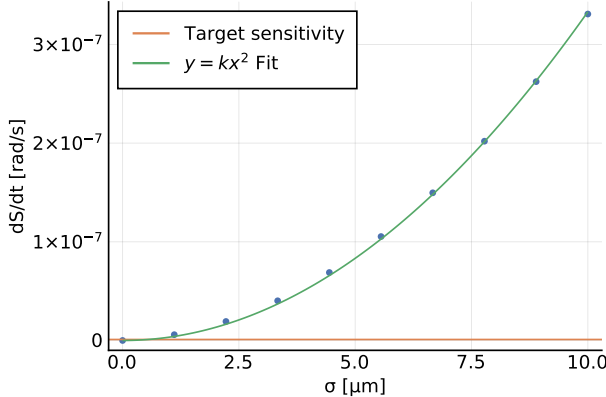


Figure 11: Vertical spin precession rate vs σ quadrupole misalignments. $\sigma = 1 \mu\text{m}$ is found to be an optimal value for the alignment requirements, as the points only represent upper limit of the possible precession rate. Additional cancellation is achieved by incorporating polarity switches with CW and CCW beams.

randomly misaligning all magnetic quadrupoles by σ (both x, y) and keep increasing σ while observing the growth of the vertical precession rate. We place a single CW beam in longitudinal polarization and observe its spin precession rate against σ . We find that (Figure 11) in order for the true EDM signal to be above the background we require around $\sigma = 1 \mu\text{m}$ for quadrupole positioning because some additional cancellation is achieved by incorporating both CW and CCW beams with opposite quadrupole polarities.

3.4 Geometrical Phase — Bending Sections

Geometrical Phase due to misalignment of the bending sections has same underlying principles but originates due to electric field. Radially polarized S_x beams happen to be the most sensitive to this. Naturally, longitudinal polarization will also be affected indirectly through some non-zero radial spin component. Assuming the ring to be aligned mechanically to 0.1 mm and 0.1 mrad we will create the worst case resonance by radially misaligning and tilting some of the deflectors as shown in Figure 12. This creates huge precession rates in both CW and CCW beams and opposite quad polarities Figure 13.

This is a major systematic effect that manifests itself prominently in radial polarization direction. Remediation to this systematic is to use radially polarized beams to reduce the misalignments in the bending plates. Vertical precession rates in radially polarized beams will be used as a feedback for the alignment of the bending sections. Hence, the alignment using spin precession is coined as “Spin-based alignment” in this discussion.

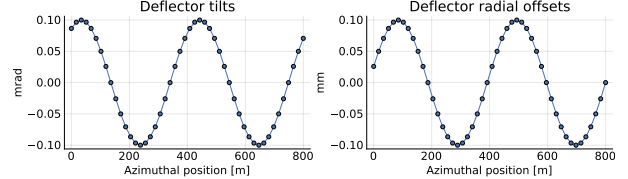


Figure 12: Deflectors are radially misaligned and tilted to create a $N=2$ spin resonance.

Radial polarization direction should be used for this particular case where it is few orders of magnitude more sensitive to geometrical phase originating from bending plates. By using Spin-based alignment using radial spin components and by observing the deviation from its ideal position (Figures 15 and 16), we expect the bending plates to be aligned to 0.01 mm and 0.01 mrad which is sufficient enough as the geometrical phase effect scales as the product of misalignments. By achieving this level of alignment, background spin precession rate drops to $dS_y/dt \approx 95 \mu\text{rad/s}$ in radial polarization case. This is well enough as longitudinal polarization is few orders of magnitude less sensitive to this effect.

In general, Spin-based alignment is not restricted to having a radial polarization direction as a feedback system for leveling the ring elements. Other systematics or ring alignment issues could be addressed using radial, longitudinal or vertical spin directions.

4 Conclusions

Most of the important systematic issues in proton storage ring EDM experiment are covered. This paper has introduced novel methods of improving the sensitivity of the experiment such as, symmetric ring design and Spin-based alignment. The storage ring proton EDM experiment aims to measure the dipole moment to $10^{-29} e\cdot\text{cm}$ with proposed improvements to the experimental technique.

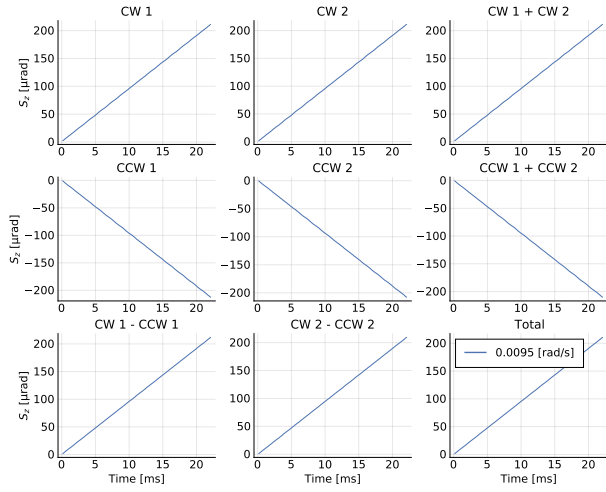


Figure 13: Vertical spin component vs. time in radially polarized beams for misalignment of deflectors at 0.1 mm and 0.1 mrad. Numbers 1,2 correspond to quad polarities. Signals from opposite directions (CW-CCW) should be subtracted and signals from opposite quad polarities 1,2 should be added to isolate true EDM signal. The background spin precession rate is not canceled with opposite quad polarities or CW - CCW beams.

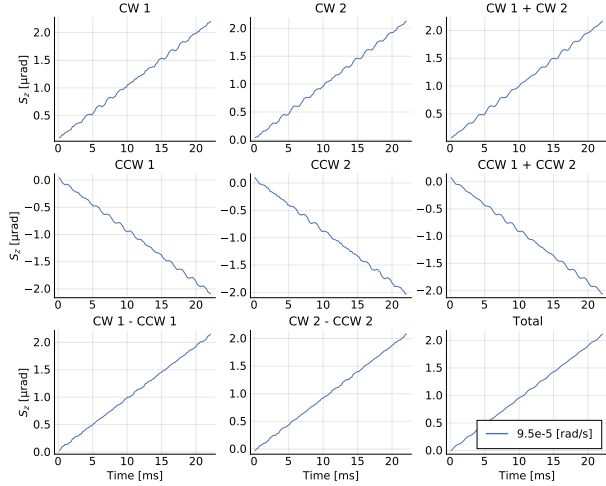


Figure 14: Vertical spin component vs. time in radially polarized beams for misalignment of deflectors at 0.01 mm and 0.01 mrad. Numbers 1,2 correspond to quad polarities. Signals from opposite directions (CW-CCW) should be subtracted and signals from opposite quad polarities 1,2 should be added to isolate true EDM signal. The background spin precession rate is not canceled with opposite quad polarities or CW - CCW beams.

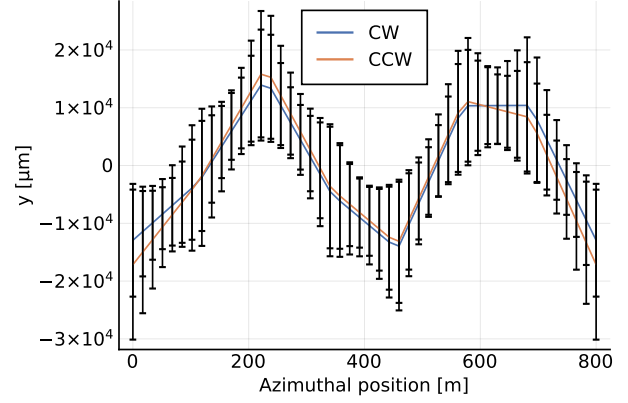


Figure 15: Vertical positions of CW and CCW beams vs. azimuthal position in the storage ring. Deflectors are misaligned as in Figure 12 with the amplitude of 0.1 mm, mrad

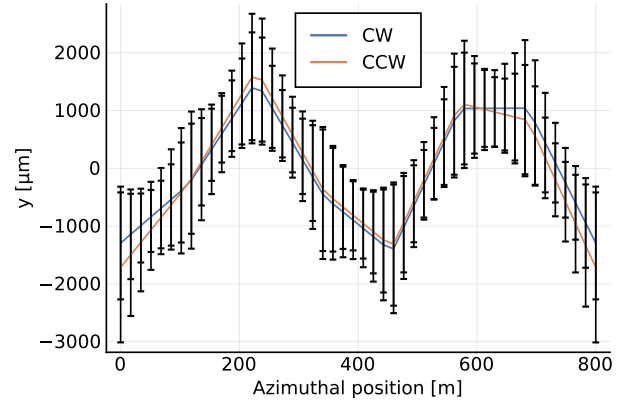


Figure 16: Vertical positions of CW and CCW beams vs. azimuthal position in the storage ring. Deflectors are misaligned as in Figure 12 with the amplitude of 0.01 mm, mrad

References

- ¹V. Anastassopoulos, S. Andrianov, R. Baartman, S. Baessler, M. Bai, J. Benante, M. Berz, M. Blaskiewicz, T. Bowcock, K. Brown, B. Casey, M. Conte, J. D. Crnkovic, N. D'Imperio, G. Fanourakis, A. Fedotov, P. Fierlinger, W. Fischer, M. O. Gaisser, Y. Giomataris, M. Grosse-Perdekamp, G. Guidoboni, S. Haciömeroğlu, G. Hoffstaetter, H. Huang, M. Incagli, A. Ivanov, D. Kawall, Y. I. Kim, B. King, I. A. Koop, D. M. Lazarus, V. Lebedev, M. J. Lee, S. Lee, Y. H. Lee, A. Lehrach, P. Lenisa, P. L. Sandri, A. U. Lucchio, A. Lyapin, W. MacKay, R. Maier, K. Makino, N. Malitsky, W. J. Marciano, W. Meng, F. Meot, E. M. Metodiev, L. Miceli, D. Moricciani, W. M. Morse, S. Nagaitsev, S. K. Nayak, Y. F. Orlov, C. S. Ozben, S. T. Park, A. Pesce, E. Petrakou, P. Pile, B. Podobedov, V. Polychronakos, J. Pretz, V. Ptitsyn, E. Ramberg, D. Raparia, F. Rathmann, S. Rescia, T. Roser, H. K. Sayed, Y. K. Semertzidis, Y. Senichev, A. Sidorin, A. Silenko, N. Simos, A. Stahl, E. J. Stephenson, H. Ströher, M. J. Syphers, J. Talman, R. M. Talman, V. Tishchenko, C. Touramanis, N. Tsoupas, G. Venanzoni, K. Vetter, S. Vlassis, E. Won, G. Zavattini, A. Zelenski, and K. Zioutas, “A storage ring experiment to detect a proton electric dipole moment”, *Review of Scientific Instruments* **87**, 115116 (2016).
- ²S. Haciomeroglu and Y. K. Semertzidis, “A hybrid ring design in the storage-ring proton electric dipole moment experiment”, arXiv:1806.09319 [physics] (2018).
- ³C. Tsitouras, “Runge–kutta pairs of order 5(4) satisfying only the first column simplifying assumption”, *Computers & Mathematics with Applications* **62**, 770–775 (2011).
- ⁴J. D. Jackson, *Classical electrodynamics 3rd edition* (John Wiley & Sons, 2007).
- ⁵M. V. Berry, “Quantal Phase Factors Accompanying Adiabatic Changes”, *Proceedings of the Royal Society of London Series A* **392**, 45–57 (1984).
- ⁶C. A. Baker, D. D. Doyle, P. Geltenbort, K. Green, M. G. D. van der Grinten, P. G. Harris, P. Iaydjiev, S. N. Ivanov, D. J. R. May, J. M. Pendlebury, J. D. Richardson, D. Shiers, and K. F. Smith, “Improved experimental limit on the electric dipole moment of the neutron”, *Phys. Rev. Lett.* **97**, 131801 (2006).
- ⁷J. M. Pendlebury, W. Heil, Y. Sobolev, P. G. Harris, J. D. Richardson, R. J. Baskin, D. D. Doyle, P. Geltenbort, K. Green, M. G. D. van der Grinten, P. S. Iaydjiev, S. N. Ivanov, D. J. R. May, and K. F. Smith, “Geometric-phase-induced false electric dipole moment signals for particles in traps”, *Phys. Rev. A* **70**, 032102 (2004).